ChemComm

Accepted Manuscript

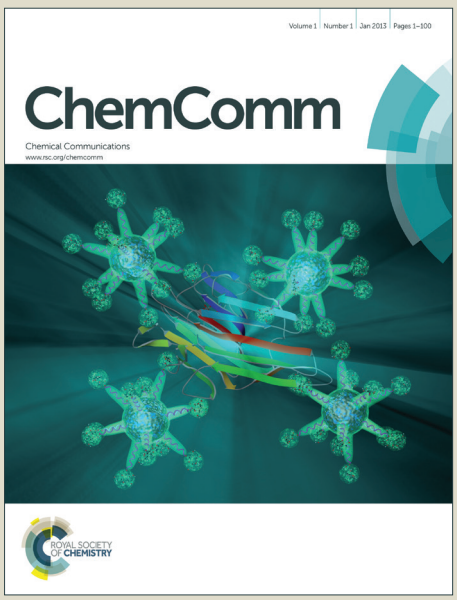

ROYAL SOCIETY OF CHEMISTRY

www.rsc.org/chemcomm

Journal Name

ARTICLE

Are the Orientation and Bond Strength of the $RCO_2^{-}\cdots M$ Link Key Factors for Ultrafast Electron Transfers?

Received 00th January 20xx,
Accepted 00th January 20xx

DOI: 10.1039/x0xx00000x

www.rsc.org/

Peng Lu,[a] Paul-Ludovic Karsenti,[a] Gessie Brisard,[a] Benoit Marsan[b] and Pierre D. Harvey[a]

The photo-induced electron transfers in the straight up ionic assemblies $[Pd_3^{2+}]\cdots$MCP and $[Pd_3^{2+}]\cdots$DCP$\cdots[Pd_3^{2+}]$ ($[Pd_3^{2+}]^* \rightarrow$ MCP or DCP) are ultrafast (< 85 fs) indicating that it is not necessary to have a strong coordination bond or a bent geometry to obtain fast electron transfer.

Porphyrins are heavily investigated for dye sensitized solar cell (DSSC) applications notoriously in their "push-pull" versions.[1] Numerous issues concerning the fast electron injection from the excited dye to the TiO_2 nanoparticles were raised. For examples, the use of carboxylates *vs* phosphates, directly comparing their interactions with Ti^{4+},[1c,2] and the presence of J-aggregates,[3] were recently debated parameters. It also became clear that the DSSCs efficiency depends not only on the rate of electron injection but also on the relative amount of dyes deactivating without electron transfer.[4] This rate is predictably distance-dependent between the dye and TiO_2 center,[5] which also contribute in retarding the competing charge recombination.[6] Moreover, recent studies also showed that the binding geometry plays a determining role on the electron transfer rate, k_{et}.[7] The current belief is that a strong O-Ti coordination bond and a bent conformation of the dye over the TiO_2 surface promote ultrafast k_{et}. The typically reported k_{et}'s are in the fs-ps time scale,[2-7] going as low as < 50 fs (*i.e.* the time resolution limit).[8] To accurately define all parameters that lead to fast electron injection, it now appears necessary to examine weakly bonded models with a "straight up" geometry; two seemingly unfavourable parameters. In such cases, k_{et} should be significantly slower (long ps). In this respect, the easily reducible unsaturated $Pd_3(dppm)_3(CO)^{2+}$ cluster (**$[Pd_3^{2+}]$**; dppm = $Ph_2PCH_2PPh_2$; Chart 1; $E^{0/-1}$ ~-0.50 V *vs* SCE as $CF_3CO_2^{-}$ salt in various solvents)[9] is an appropriate model as it weakly binds carboxylate ions "straight up" above the Pd_3 plane strictly *via* ionic interactions (based on X-ray data using $CF_3CO_2^{-}$ ions).[10] This geometry is favoured *via* host-guest interactions of the RCO_2^{-} group inside the cavity formed by the phenyls of the dppm ligands above the M_3 frame.

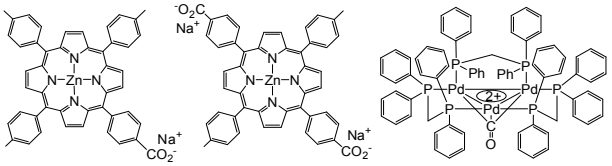

Scheme 1. Structures of **MCP**, **DCP** and **$[Pd_3^{2+}]$** (as PF_6^{-} salt).

Despite the expectation for a slow rate, we now report that the photo-induced electron transfers for the **$[Pd_3^{2+}]$•••MCP** and **$[Pd_3^{2+}]$•••DCP•••$[Pd_3^{2+}]$** assemblies (**MCP**, **DCP** = 5-(4-carboxylphenyl)-10, 15, 20-tristolyl(porphyrinato)zinc(II), 5, 15-bis(4-carboxylphenyl)-15, 20-bistolyl(porphyrinato)zinc(II), respectively; as Na^+ salts; Scheme 1) are in fact also ultrafast (< 85 fs).

The host-guest assemblies (eqs. 1 and 2) are generated in MeOH solutions easily monitored by UV-vis spectroscopy (detail in ESI). The binding constants, K_{11} and K_{12}, were extracted using the Scatchard, Scott and Benesi-Hilderbrand plots.[11,12] The K_{11} and K_{12} values for the sequential formation of **$[Pd_3^{2+}]$•••DCP** and **$[Pd_3^{2+}]$•••DCP•••$[Pd_3^{2+}]$** are reasonably assumed to be the same as no slope change in the low and high concentration range of **$[Pd_3^{2+}]$** was detected. This effect is consistent with the absence of steric hindrance. The similarity of the 19300 and 22000 M^{-1} constants readily attests this assumption.

$$[Pd_3^{2+}] + \text{MCP} \rightleftharpoons [Pd_3^{2+}]\bullet\bullet\bullet\text{MCP} \qquad K_{11} = 19300\ M^{-1} \quad (1)$$

$$2\,[Pd_3^{2+}] + \text{DCP} \rightleftharpoons [Pd_3^{2+}]\bullet\bullet\bullet\text{DCP}\bullet\bullet\bullet[Pd_3^{2+}] \qquad K_{12} = 22000\ M^{-1} \quad (2)$$

Previous X-ray data indicated a "straight up" geometry of the $CF_3CO_2^{-}\bullet\bullet\bullet M_3$ unit with ionic Pd•••O distances of 2.57 to 3.06 Å with the CO_2 unit placed closer to one of the Pd-Pd bond.[10] In the absence of X-ray data, the optimized geometries of the assemblies were calculated using DFT and confirmed the expected geometry (Figure 1; see ESI for **$[Pd_3^{2+}]$•••DCP•••$[Pd_3^{2+}]$**). The computed "gas phase" Pd•••O distances ranging from 2.411 to 3.368 Å are also consistent with ionic interactions.

[a] *Département de chimie, Université de Sherbrooke, Sherbrooke, QC, J1K 2R1, Canada.*
[b] *Département de chimie, Université du Québec à Montréal, Montréal, QC, H2X 2J6, Canada.*

† *Electronic Supplementary Information (ESI) available: Experimental section, binding constant analyses, DFT and TDDFT, TAS kinetic and photophysical data. See DOI: 10.1039/x0xx00000x*

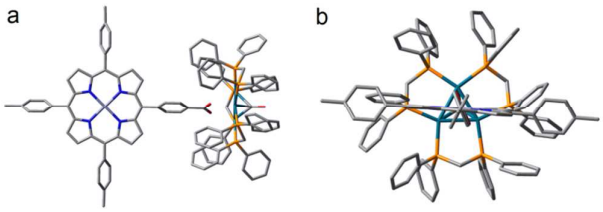

Figure 1. Side (a) and top (b) views of the optimized geometry (DFT) of the **[Pd_3^{2+}]•••MCP** host guest assembly (ground state). Pd•••O distances: 1st O; 3.368, 3.298, 2.416, 2nd O; 3.516, 3.175, 2.411 Å. The O-atoms (red) are placed more closely above a Pd-Pd bond rather of being in the center. For **[Pd_3^{2+}]•••DCP•••[Pd_3^{2+}]**, see ESI.

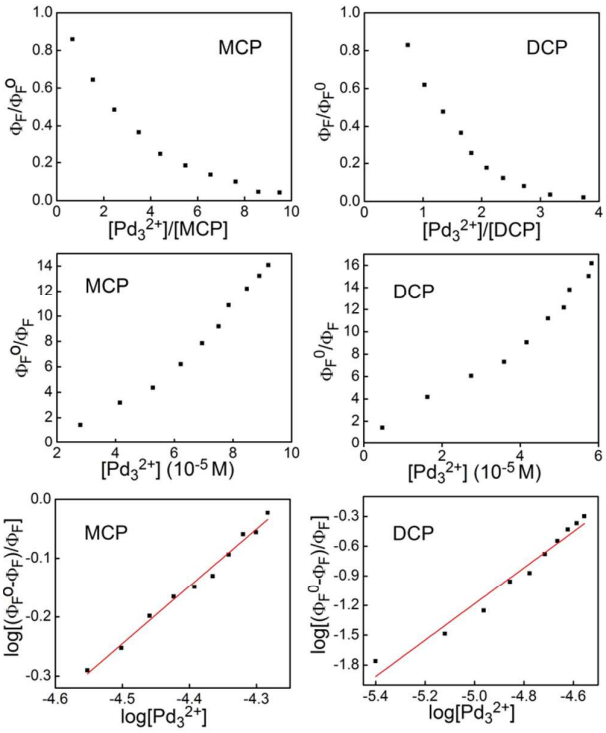

Figure 2. Top: graphs reporting the decrease of the relative fluorescence intensity of **MCP** and **DCP** upon addition of **[Pd_3^{2+}]** (Φ_F and Φ_F° are the intensity in the presence and absence of **[Pd_3^{2+}]**, respectively). Middle: Stern-Volmer plots of the fluorescence quenching of **MCP** and **DCP** by **[Pd_3^{2+}]**. Bottom: graph reporting $\log[(\Phi_F°-\Phi_F)/\Phi_F]$ vs log**[Pd_3^{2+}]**. The red lines are the best fits allowing extracting n.

The **MCP** and **DCP** fluorescence bands exhibit quenching upon addition of **[Pd_3^{2+}]** (Figure 2; top) but the fluorescence lifetimes remain constant (ESI) indicating the presence of static quenching (*i.e.* the free dyes and assemblies are emissive and non-emissive, respectively). The lack of linearity in the Stern-Volmer plots (Figure 2; middle) corroborates this conclusion. In such a case, the data are analyzed using the relation $\log[(\Phi_F°-\Phi_F)/\Phi_F] = \log(K_b) + (n \bullet \log[\mathbf{Pd_3^{2+}}])$ where Φ_F° and Φ_F are the fluorescence intensities in respectively the absence and presence of **[Pd_3^{2+}]**, K_b is the binding constant, and n is the average number of binding sites (Figure 2; bottom).[13] Values of n = 0.97 (**MCP**) and 1.83 (**DCP**) are obtained, which are consistent with the number of carboxylates on the dyes.

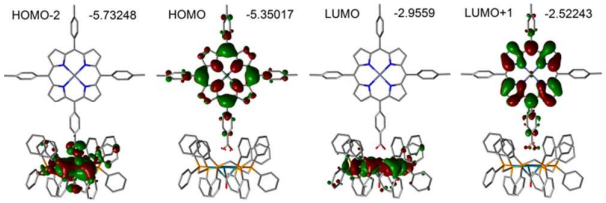

Figure 3. Selected frontier MO representations of **[Pd_3^{2+}]•••MCP** (in eV; see ESI for **[Pd_3^{2+}]•••DCP•••[Pd_3^{2+}]** and for the HOMO-1 (**MCP** π-level)).

Table 1. K_D, V and n data for the assemblies (solvent = MeOH at 298 K, and MeOH/2MeTHF 1:1 at 77 K).

assemblies (temperature)	n	K_D (M^{-1})	V (M^{-1})
[Pd_3^{2+}]•••MCP (298 K)	0.97	241	17900
[Pd_3^{2+}]•••DCP•••[Pd_3^{2+}] (298 K)	1.83	2750	21300
[Pd_3^{2+}]•••MCP (77 K)	0.91	3400	21900
[Pd_3^{2+}]•••DCP•••[Pd_3^{2+}] (77 K)	2.10	3700	25800

Table 2. Relative percentage of complexed dyes *vs* the $[CO_2^-]$/**[Pd_3^{2+}]** ratio.

$[CO_2^-]$/ **[Pd_3^{2+}]**	K_{11}, V (in $[M]^{-1}$)	K_{12}, V (in $[M]^{-1}$)
1:1	**[Pd_3^{2+}]•••MCP** 22.1, 21.1	**[Pd_3^{2+}]•••DCP** 28.0, 28.0
		([Pd_3^{2+}])$_2$•••DCP 13.3, 12.7
1:2	**[Pd_3^{2+}]•••MCP** 37.4, 35.8	**[Pd_3^{2+}]•••DCP** 33.3, 33.3
		([Pd_3^{2+}])$_2$•••DCP 32.7, 32.0
1:4	**[Pd_3^{2+}]•••MCP** 55.8, 54.2	**[Pd_3^{2+}]•••DCP** 21.3, 28.0
		([Pd_3^{2+}])$_2$•••DCP 72.0, 58.7

In order to verify whether the quenching is dominantly static, a mixed dynamic-static model was used,[14] which is derived from a sphere of action quenching model: $[1-(\Phi_F-\Phi_F°)]/[\mathbf{Pd_3^{2+}}] = K_D \bullet (\Phi_F/\Phi_F°) + (1-W)/[\mathbf{Pd_3^{2+}}]$ where W is the fraction of the excited-state quenching from a collisional process given by $\exp(-V \bullet [\mathbf{Pd_3^{2+}}])$ (V is the static quenching constant representing the volume of the sphere of action) and K_D is the dynamic quenching constant. From a plot $[1-(\Phi_F-\Phi_F°)]/[\mathbf{Pd_3^{2+}}]$ *vs* $(\Phi_F/\Phi_F°)$, K_D is extracted from the slope using a least-square fit (ESI) and the intercept leads to the W values as a function of **[Pd_3^{2+}]**. Then V is evaluated from the slopes in the ln(W) *vs* **[Pd_3^{2+}]** plots (ESI). These values are K_D = 241 and V = 17900 for **[Pd_3^{2+}]•••MCP** and K_D = 2750 $[M]^{-1}$ and V = 21300 $[M]^{-1}$ for **[Pd_3^{2+}]•••DCP•••[Pd_3^{2+}]**. Because the V values are much larger than those for K_D, the static quenching dominates the overall mechanism, and unsurprisingly, K_{11} and K_{12} are similar to V. In order to confirm this conclusion, this same analysis was performed on the assemblies' fluorescence at 77 K (*i.e.* only static quenching is possible). Indeed, the same relationship (*i.e.* K_D < V) is observed (Table 1, and all graphs are placed in the ESI). The K_{11}, K_{12} and K_D constants are then employed to evaluate of the proportion of molecular complexes at various CO_2^-/**[Pd_3^{2+}]** ratios (Table 2), which is useful for the interpretation of the fs transient absorption spectra (TAS) below.

Both the **MCP** and **DCP** dyes exhibit irreversible oxidation and reduction waves in the cyclic voltammograms, CV (ESI). **MCP** is slightly harder to oxidize and easier to reduce compared to **DCP** (Table 3) which is consistent with their number of negative charges. Concurrently, **[Pd_3^{2+}]** exhibits oxidation and reduction potentials at $E^{0/+1}$ = +0.95 V[15] and $E^{0/-1}$ = -0.50 V *vs* SCE.[9]

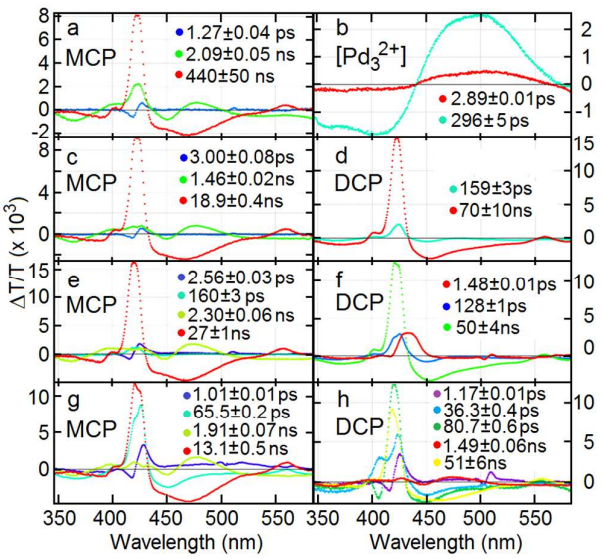

Figure 4. Individual components extracted from fs TAS (λ_{exc}= 600 nm, MeOH, 298 K) with CO_2^{-}/[Pd_3^{2+}] ratios for MCP of 1:0 (a), 1:1 (c) 1:2 (e), and 1:4 (g) and for DCP of 1:0 (d), 1:1 (f) and 1:2 (h), and [Pd_3^{2+}] (b). The transient and bleach signals are respectively below and above the zero line.

Using the 0-0 peak position of the Q band (600 nm; 2.07 eV), the S_1 driving forces for the oxidative (+1.57 V) and reductive quenching (-1.12 V *vs* SCE) can be extracted as well as ΔGs for ***donor***•••**[Pd$_3^{2+}$]*** → ***donor***$^{\bullet+}$***••• [Pd$_3^{\bullet+}$]*** (+0.67; **MCP**, +0.72 V *vs* SCE; **DCP**), and for ***acceptor*** •••**[Pd$_3^{2+}$]*** → ***acceptor***$^{\bullet-}$***•••[Pd$_3^{3+}$]*** (+0.38; **MCP**, +0.32 V *vs* SCE; **DCP**). Thermodynamically, the oxidative quenching of the dyes is more favorable than the reductive one. In order to coroborate this conclusion, DFT computations were performed in order to obtain their MO representations and energies of the frontier MOs (Figure 3 and ESI). For instance, the **[Pd$_3^{2+}$]•••MCP** assembly exhibits a HOMO and LUMO+1 that are typical π-MO for a chromophore. Concurrently, the HOMO-2 and LUMO are respectively the first filled and empty d orbitals of the Pd_3 frame. Importantly, these levels are clearly energetically well isolated from one another (> ~0.4 eV) and so the oxidation and reduction processes can only take place in the porphyrin and cluster units, respectively.

As the assemblies are non-emissive due to the oxidative quenching of the excited dyes by **[Pd$_3^{2+}$]**, TAS was used to extract k_{et}. First, these units are investigated separately to obtain their spectral and kinetic signatures (Figure 4a, b, d). The **MCP** and **DCP** TAS are characterized by the appearance of a broad transient signal (430-530 nm) and a strong bleach of the Soret band (425). The deconvolution of the data allows for the extraction of the various components and lifetimes. The strong and long ns-components (440 and 70 ns, respectively) are triplet species (T_1) but their lifetimes are simply considered inaccurate due to the delay line of only 3.3 ns. Indeed, the previously reported T_1 value for **MCP** in 2MeTHF is 137 μs (without O_2).[16] For the singlet species, S_1, the signals are weak. The ~2.1 ns component in **MCP** is clearly the S_1 emissive species (τ_F = 1.97 ± 0.08 ns), but it is not observed for **DCP** (τ_F = 2.04 ± 0.10 ns; note that a signal with a lifetime of ~1.5 ns is detected in Figure 4f,h and is likely to be this species). This absence is due to the weakness of this signal compared to the dominant triplet species.

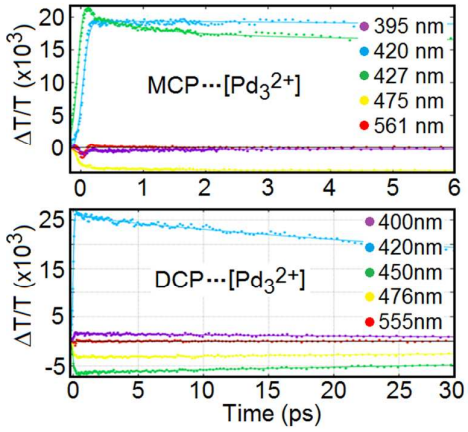

Figure 5. Monitoring of the TAS of MCP and DCP in the presence of [Pd_3^{2+}] in MeOH using CO_2^{-}/[Pd_3^{2+}] ratios of 1:4 and 1:2, respectively. The pulse width of the laser pulse is 85 fs and no rise time is observed.

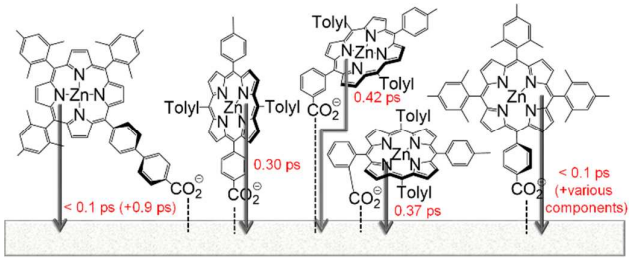

Figure 6. Some examples of time scales for electron injection of various mono-carboxylates of zinc(II)porphyrin into TiO_2 nanoparticles.[7a,c]

The ps-components are the known non-emissive species Zn(porphyrin)•••solvent.[17] No exhaustive study was performed on these species since this was not the aim of this investigation. Concurrently, the **[Pd$_3^{2+}$]** TAS exhibit two components (~2.9 and 296 ps) with practically identical signatures (Figure 4b). These are tentatively assigned to S_1 and T_1 species. The exact knowledge of these species is a minor issue in this work since these signals are not observed in the TAS of the assemblies (Figure 4). This situation is likely due to the weakness of the signal relative to those of the dyes. The TAS *vs* the CO_2^{-}**/[Pd$_3^{2+}$]** ratios allow for the reliable detection of the signals associated with the assemblies **[Pd$_3^{\bullet+}$]•••MCP**$^{\bullet+}$ and **[Pd$_3^{\bullet+}$]•••DCP**$^{\bullet+}$**•••[Pd$_3^{2+}$]**. Upon increasing these ratios new signals with different shapes and lifetimes appear and are readily assigned to these charge separated species. Noteworthy, if the quenching was due to S_1 energy transfer, the band shape of the transient signals would be constant, which is clearly not the case. For **MCP**, this distinctive signal is the one with lifetimes respectively of 160 and 65.5 ps (Figure 4e,g). Because its signal is expectedly stronger for the 1:4 ratio (Figure 4g), both its band shape and lifetime are more reliable (and used for the extraction of k_{et}). For **DCP**, this distinctive signal is the one with a lifetime of 36.3 ps (Figure 4h).

Normally k_{et} is reliably obtained from the rise times monitored at wavelengths where their signals are stronger. However, no rise time longer than the pulse width was detected (for all monitoring wavelengths in fact) indicating that all species are formed during the laser pulse (< 85 fs; Figure 5), including the charge separated **[Pd$_3^{\bullet+}$]•••MCP**$^{\bullet+}$ and **[Pd$_3^{\bullet+}$]•••DCP**$^{\bullet+}$**•••[Pd$_3^{2+}$]** species. Therefore k_{et} must be > 1.2 x 10^{13} s^{-1}, which is clearly an ultrafast event.[18] This

time scale also compares favorably to what is commonly encountered for other zinc(II)porphyrins linked to the surface of TiO_2 nanoparticles (Figure 6; this list is far from exhaustive but is representative). However, this value can also be considered to be on the fast side. Similarly, the charge recombination characterized by TAS decays here found in the order of ~36 and ~66 ps, which also fall in the range of what it is currently reported.[7]

The ultrafast photo-induced electron transfers ($k_{et} > 1.2 \times 10^{13}$ s^{-1}) occurring at the S_1 levels of the dyes in the structurally well-defined "straight up" ionic assemblies clearly indicate that it is not necessary to have a strong bond between the donor and acceptor and have a bent geometry.

Acknowledgements

This research was supported by the Fond de Recherche Québécois sur la Nature et la Technologie (FRQNT), and the Centre Québécois des Matériaux Fonctionnels (CQMF).

Notes and references

1 (a) R. L. Milot and C. A. Schmuttenmaer. *Acc. of Chem. Res*. 2015, **4**8, 1423. (b) T. Higashino and H. Imahori. *Dalton Trans*. 2015, **44**, 448. (c) C. Stern, A. Bessmertnykh Lemeune, Y. Gorbunova, A. Tsivadze, and R. Guilard. Turkish J. Chem. 2014, 38, 980. (d) K. Ladomenou, T. N. Kitsopoulos, G. D. Sharma, and A. G. Coutsolelos. RSC Advances 2014, 4, 21379. (e) E. W.-G. Diau and L.-L. Li, Eds. K. M. Kadish, K. M. Smith, R. Guilard, *Handbook of Porphyrin Science* 2014, **28**, 279. (f) L. Giribabu, and R. K. Kanaparthi, *Curr. Sci.* 2013, **104**, 847. (g) M. K. Panda, K. Ladomenou, and A. G. Coutsolelos. *Coord. Chem. Rev*. 2012, **256**, 2601. (h) M. V. Martinez-Diaz, G. de la Torre, and T. Torres. *Chem. Commun*. 2010, **46**, 7090. (i) X. Li, H. Wang, and H. Wu, Haixia. *Structure and Bonding* 2010, **135**, 229. (j) X.-F. Wang, and H. Tamiaki. *Ener. Env. Sci.* 2010, **3**, 94. (k) W. M. Campbell, A. K. Burrell, D. L. Officer, and K. W. Jolley. *Coord. Chem. Rev*. 2004, **248**, 1363. (l) M. J. Griffith, K. Sunahara, P. Wagner, K. Wagner, G. G. Wallace, D. L. Officer, A. Furube, R. Katoh, S. Mori and A. J. Mozer. *Chem. Commun*., 2012, **48**, 4145.

2 B. J. Brennan, M. J. Llansola Portoles, P. A. Liddell, T. A. Moore, A. L. Moore, and D. Gust. *Phys. Chem. Chem. Phys*. 2013, **15**, 16605.

3 (a) S. Verma, A. Ghosh, A. Das, and H. N. Ghosh. *Chem. Eur. J*. 2011, **17**, 3458. (b) S. Verma and H. N. Ghosh. *J. Phys. Chem. Lett*. 2012, **3**, 1877.

4 K. Sunahara, A. Furube, R. Katoh, S. Mori, M. J. Griffith, G. G. Wallace, P. Wagner, D. L. Officer, and A. J. Mozer. *J. Phys. Chem. C* 2011, **115**, 22084.

5 C.-W. Chang, L. Luo, C.-K. Chou, C.-F. Lo, C.-Y. Lin, C.-S. Hung, Y.-P. Lee, and E. W.-G. Diau. *J. Phys. Chem. C* 2009, **113**, 11524.

6 J. Lu, Y.-C. Chang, H.-Y. Cheng, H.-P. Wu, Y. Cheng, M. Wang, and E. W.-G. Diau. *ChemSusChem* 2015, in press.

7 (a) S. Ye, A. Kathiravan, H. Hayashi, Y. Tong, Y. Infahsaeng, P. Chabera, T. Pascher, A. P. Yartsev, S. Isoda, H. Imahori, and V. Sundström. *J. Phys. Chem. C* 2013, **117**, 6066. (b) H. Imahori, S. Kang, H. Hayashi, M. Haruta, H. Kurata, S. Isoda, S. E. Canton, Y. Infahsaeng, A. Kathiravan, T. Pascher, P. Chabera, A. P. Yartsev, and V. Sundström, *J. Phys. Chem. A* 2011, **115**, 3679. (c) A. S. Hart, C. B. KC, H. B. Gobeze, L. R. Sequeira, and F. D'Souza. *ACS Appl. Mater. Interfaces* 2013, **5**, 5314.

8 M. R. di Nunzio, B. Cohen, S. Pandey, S. Hayse, G. Piani, and A. Douhal, *J. Phys. Chem. C* 2014, **118**, 11365.

9 I. Gauthron, Y. Mugnier, K. Hierso, and P. D. Harvey. *Can. J. Chem*. 1997, **75**, 1182.

10 (a) R. Provencher, K. T. Aye, M. Drouin, J. Gagnon, N. Boudreault, and P. D. Harvey. *Inorg. Chem*. 1994, **33**, 3689. (b) C. Salomon, D; Fortin, C. Darcel, S. Juge, and P. D. Harvey. *J. Cluster Sci.* 2009, **20**, 267.

11 K. A. Connors. Binding Constants: The Measurements of Molecular Complex Stability. Wiley & Sons, New York, 1987.

12 B. Du, C. Stern, and P. D. Harvey, *ChemComm* 2011, **47**, 6072.

13 M. Makarska-Bialokoz. *J. Luminescence* 2014, **147**, 27.

14 M. Acar, E. Bozkurt, K. Meral, M. Arık, and Y. Onganer, *J. Luminescence* 2015, **157**, 10.

15 D. Brevet, D. Lucas, Y. Mugnier, and P. D. Harvey. *J. Clus. Sci*. 2006, **17**, 5.

16 S. M. Aly, C. Ayed, C. Stern, R. Guilard, A. S. Abd-El-Aziz, and P. D. Harvey. *Inorg. Chem.* 2008, **47**, 9930-9940.

17 H.-Z. Yu, J. S. Baskin, and A. H. Zewail, *J. Phys. Chem. A* **2002**, *106*, 9845.

18 P. D. Harvey. Eds K. M. Kadish, R. Guilard and K. M. Smith *Handbook of Porphyrin*, Elsevier, 2003, **113**, 63.